Tissue Engineering

DOI: 10.1089/ten.TEC.2019.0088

An Air Bubble-Isolating Rotating Wall Vessel Bioreactor for Improved Spheroid/Organoid Formation

MICHAEL A. PHELAN, ANTHONY L. GIANFORCARO, JONATHAN A. GERSTENHABER, AND PETER I. LELKES

INTEGRATED LABORATORY FOR CELLULAR TISSUE ENGINEERING AND REGENERATIVE MEDICINE, DEPARTMENT OF BIOENGINEERING, COLLEGE OF ENGINEERING, TEMPLE UNIVERSITY, PHILADELPHIA, PA, USA

CORRESPONDENCE TO:

Peter I. Lelkes, PhD

Fellow, American Institute for Medical & Biological Engineering

Laura H. Carnell Professor and Chair, Dept. Bioengineering, College of Engineering

Temple University

Engineering Building Room 811

1947 N. 12th Street

Philadelphia, PA 19122

Dept. Website: http://engineering.temple.edu/department/bioengineering

Tel: +1 215-204-3307

FAX: +1 215-204-3226

email: pilelkes@temple.edu

Running Title: *A Novel Air Bubble-Isolating Rotating Wall Vessel Bioreactor*

Tissue Engineering
An Air Bubble-Isolating Rotating Wall Vessel Bioreactor for Improved Spheroid/Organoid Formation (DOI: 10.1089/ten.TEC.2019.0088)
This paper has been peer-reviewed and accepted for publication, but has yet to undergo copyediting and proof correction. The final published version may differ from this proof.

ABSTRACT

Rotating wall vessel (RWV) bioreactors have been used to produce cell spheroids and organoids at a faster rate than in other bioreactor devices and with higher structural and functional fidelity. One of the limitations of traditional RWV systems is the well-documented tendency for air bubble formation during operation. The presence of these bubbles negates key features of the RWV environment, such as zero headspace, low-shear, and simulated microgravity. In this paper, we describe the design, construction, and testing of a novel RWV capable of constantly removing air bubbles from the system without interfering with the fluid dynamics that produce optimized cell culture conditions. We modeled this capacity using computational fluid dynamics (CFD) and then validated the model with alginate beads and spheroid cultures of A549 human lung adenocarcinoma cells. The areas of spheroids assembled from A549 cells in the novel bioreactor in the presence of air bubbles were an order of magnitude larger than in conventional bioreactors when bubbles were present. Our results demonstrate the ability of the novel design to remove and isolate bubbles while avoiding damage to spheroid assembly, as observed in conventional RWV bioreactors in the presence of bubbles. We anticipate that the novel design will increase experimental reproducibility and consistency when using rotating wall vessel bioreactors.

IMPACT STATEMENT

The rotating wall vessel (RWV) bioreactor is a powerful tool for the generation of sizeable, faster-growing organoids. However, the ideal, low-shear, modeled microgravity environment in the RWV is frequently disrupted by the formation of bubbles, a critical but understated failure mode. To address this, we have designed and fabricated a novel, modified RWV bioreactor capable of continuously removing bubbles while providing optimal fluid dynamics. We validated the capacity of this device with computational and empirical studies. We anticipate that our novel bioreactor will be more consistent and easier to use and may fill a unique and unmet niche in the burgeoning field of organoids.

Keywords: Air Bubble, Computational Fluid Dynamics (CFD), High Aspect Ratio Vessel (HARV), Organoid, Rotating Wall Vessel (RWV), Modeled Microgravity

Tissue Engineering
An Air Bubble-Isolating Rotating Wall Vessel Bioreactor for Improved Spheroid/Organoid Formation (DOI: 10.1089/ten.TEC.2019.0088)
This paper has been peer-reviewed and accepted for publication, but has yet to undergo copyediting and proof correction. The final published version may differ from this proof.

INTRODUCTION

Organoids and Spheroids in Rotating Wall Vessel (RWV) Bioreactors: 2D cell culture, the gold standard of *in vitro* biology for nearly a century, has been used in virtually every major discovery in cell biology. However, increasing understanding of the complexity of biological systems has led to heightened awareness of the importance of model systems that more closely replicate the true 3D environment of living tissues.[1] While extensive progress has been made in engineered 3D scaffolds, organ recellularization, and bioprinting, recent studies demonstrate the unique potential of self-assembling spheroids and organoids for discoveries in disease modeling, drug discovery, and a host of other biomedical applications.[2]

Although several protocols exist for the generation and maintenance of spheroids and organoids such as spontaneous self-assembly in non-adherent cell culture plates[3] or the hanging drop method,[4] culturing cells in the RWV bioreactor, with its improved nutrient exchange, yields consistent formation of organoids with superior morphology and unique, organotypic gene expression.[5–11] The RWV bioreactor works by slowly rotating a liquid-filled cylinder on its axis, gently dragging the fluid, and any particles in it, in perfect circular paths. While alternate systems, like stirred-tank bioreactors, are also being used and optimized for organoid generation with high mass transfer[12] the RWV, with its lack of impellors or agitators, produces a lower shear, lower turbulence environment, reducing potential damage to forming tissues.[13] This unique environment continues to provide high mass transfer associated with increased metabolic activity,[14] altered differentiation with increased nutrient availability,[15] modulation of pluripotency markers such as Oct4 linked to glycolytic enzymes such as pyruvate kinases,[16] and differentiation associated with higher oxygen concentration[17] both with pluripotent and multipotent cells mediated through hypoxia-inducible factor,[18–21] In conjunction with high mass transfer, the low-shear environment of the RWV can improve culture condition of particular tissue types by eliminating detrimental shear effects, such as those driving cells toward a hematopoietic fate,[22] inducing caspase-mediated apoptosis in some cell types,[23] damaging delicate organoid substructures such as photoreceptor cilia,[24] affecting cell metabolism,[25] or simply failing to support the critical, low-shear biophysical environment required for certain types of differentiation.[26] Recently, DiStefano, et al. demonstrated that the tissue-like assembly

Tissue Engineering
An Air Bubble-Isolating Rotating Wall Vessel Bioreactor for Improved Spheroid/Organoid Formation (DOI: 10.1089/ten.TEC.2019.0088)
This paper has been peer-reviewed and accepted for publication, but has yet to undergo copyediting and proof correction. The final published version may differ from this proof.

of murine retinal organoids cultured into a tissue-like assembly with properly organized photoreceptor cells occurred significantly faster and the nascent organoids were significantly larger than in static cultures. Faster generation of larger, high-fidelity organoids in the RWV may facilitate the dissemination of these organoids for high-throughput tissue analysis in drug discovery and personalized medicine.[27,28]

Bubble Formation in the Rotating Wall Vessel Bioreactor and Its Impact: Initially developed by NASA in the 1980s, RWVs were originally designed to safely shuttle cells into space as scientists endeavored to discover the biological effects of microgravity and space radiation. However, it was quickly discovered that the RWV was also capable of supporting the formation of complex, 3D, tissue-like structures of high fidelity and relevance to biomedical research on the ground.[29]

Given that the low-shear, microgravity-simulating effect of the RWV relies on a circular, solid-body fluid path along its interior perimeter, the RWV requires a "zero headspace" condition, literally a continuous interface between the fluid and the wall with no air gap.[29,30] When this interface is disrupted due to the presence of a bubble, buoyancy continually pushes the bubble to the highest point of the system despite the rotation of the device. The presence of a bubble at this locale interrupts the fluid path, adding turbulence and fluid shear stress, as the fluid is deflected around the bubble. Bubbles are easily formed because each RWV bioreactor has a gas exchange system for cellular respiration and for balancing the cell culture media pH with incubator CO_2. When the incubator environment has insufficiently high humidity (below 100%), negative pressure can form as water vapor diffuses away from the bioreactor, inevitably causing dissolved gases to precipitate out, forming unwanted bubbles. The need to remove bubbles from the RWV system prior to and/or during use is widely discussed in literature,[7,10,30–36] including a description of the issue in RWV bioreactors in low-Earth orbit.[37] While the significance of failing to remove bubbles or an analysis of the change in shear due to the presence of a bubble is not widely discussed, it has been reported on occasion that bubble formation in the RWV may disrupt cell aggregation, decrease cell viability, and harm differentiation, subsequently harming organoid formation.[7,35,38,39] Similarly, the literature is scant on providing a consistent way of preventing bubble formation.

Tissue Engineering
An Air Bubble-Isolating Rotating Wall Vessel Bioreactor for Improved Spheroid/Organoid Formation (DOI: 10.1089/ten.TEC.2019.0088)
This paper has been peer-reviewed and accepted for publication, but has yet to undergo copyediting and proof correction. The final published version may differ from this proof.

Some authors suggest a sufficiently high humidity incubator (several water pans used simultaneously) will prevent bubble formation.[30] However, with the need to open the incubator for media changes or removal of samples at different time points, this becomes difficult to maintain in practice, resulting in the frequent formation of small bubbles within 24-48 hours, which in turn can act as nucleation points for large bubble growth. Over longer time points, such as those required for organoid differentiation, bubble formation is inevitable. Nascent bubbles formed during extended culture can be removed manually by "alternating between driving plungers" of media-filled syringes.[10] However, even short-term exposure to bubble-associated shear stress may be detrimental; genetic expression can be influenced by only minutes of exposure to elevated shear stress.[40] With the increasing use of RWV bioreactor technology for organoid research, there is a need for an improved system capable of reproducibly neutralizing the impact of incidental bubbles by automatically removing them as they are formed.

In this study, we designed and implemented a modification to the High Aspect Ratio Vessel (HARV) -type RWV, a low-volume version of the RWV, which resulted in the effective capture and removal of bubbles. Comparison between the modified and standard bioreactors showed similarities in both fluid dynamics and in the generation of organoids under ideal, non-bubble conditions. While the formation of spheroids/organoids was impaired in conventional RWVs in the presence of a bubble, it was fully maintained in the modified design.

MATERIALS AND METHODS

Bioreactor Design, Modeling, and Computational Fluid Dynamics: Potential bubble segregating designs were drawn in 2D in AutoCAD 2018 software (Autodesk, Mill Valley, CA). The final design opted for a main body, similar to that of existing RWV bioreactors, with an additional thin, exterior, concentric channel running along approximately 80% of the total perimeter and connected to the main body by a thin entrance. Conceptually, our design relies on buoyancy to continuously direct air bubbles out of the main volume into the channel. Additionally, a port added to the end of the channel aides in filling and emptying and can be used to remove bubbles during operation, ensuring long-term bubble-free culture. The volumes and dimensions of the main body were based off existing

disposable 10 ml HARV models (Synthecon, Inc., Houston, TX), while the channel was given an additional volume of approximately 3 ml.

Computational Fluid Dynamics (CFD) was employed to numerically evaluate the fluid dynamics of the new design. The "Fluent" software package (ANSYS 19.2, Ansys, Inc., Canonsburg, PA) was used to model fluid behavior in both the novel design and the existing 10 ml HARV-type RWV in a 3D environment with and without an added water vapor bubble. Unless noted otherwise, added bubbles were of a radius of 2 mm for a volume of approximately 330 µl. Additional details are described in the supplementary data section (Supplemental Figure 2).

Bioreactor Fabrication: The bubble capturing bioreactors (BCBs) were designed to be leak-proof, non-cytotoxic, sterilizable, and gas permeable for cellular respiration/pH control. Additionally, separate "control" RWVs using identical materials were constructed emulating the existing HARV-type RWV bioreactors. The two designs are referred to as "novel" or "BCB" and "standard" or "HARV-type", respectively (Figures 1A and 1D show their finished construction respectively).

All systems were primarily constructed from 3/16" cast acrylic ACRYLITE® (Evonik Industries, Essen, Germany) and cut on a VLS 6.60 laser cutting table (Universal Laser Systems, Scottsdale, AZ). A gas-permeable membrane was produced by laminating a sheet of Tegaderm® (3M, Maplewood, MN), a known watertight, gas-permeable polymer, onto a flexible nylon mesh with a 300 µm pore size (McMaster-Carr) and tightly compressing under a vice overnight to ensure bonding.[41] The nylon-mesh-backed Tegaderm® was then laser-cut to match the size and bolt holes of the acrylic pieces. Finally, a 0.5 mm-thick heat-resistant silicone sheet (Laimeisi Silicone, Ltd., Shenzhen, China) was laser-cut to match the shape of the central acrylic ring and to act as a compressible leak-resistant gasket. Stopcocks and Luer closures (McMaster-Carr) were added to enable filling. Additional information on the bioreactor fabrication can be found in the supplementary data section (Supplemental Figure 1).

Alginate Bead Fluid Dynamics Validation: To validate the predicted motion of spheroids in the bioreactors, we used low-density calcium alginate beads (approximately 2 mm in diameter). Approximately two dozen beads were loaded into both types of bioreactors with and without added air bubbles (~500 µl) to replicate ideal and failure conditions and

Tissue Engineering
An Air Bubble-Isolating Rotating Wall Vessel Bioreactor for Improved Spheroid/Organoid Formation (DOI: 10.1089/ten.TEC.2019.0088)
This paper has been peer-reviewed and accepted for publication, but has yet to undergo copyediting and proof correction. The final published version may differ from this proof.

Tissue Engineering
An Air Bubble-Isolating Rotating Wall Vessel Bioreactor for Improved Spheroid/Organoid Formation (DOI: 10.1089/ten.TEC.2019.0088)
This paper has been peer-reviewed and accepted for publication, but has yet to undergo copyediting and proof correction. The final published version may differ from this proof.

rotated at 25 rpm, a speed required for larger aggregates,[42] until each system had achieved stable fluid dynamics, as inferred from reduced motion relative to any fixed position on the device. Motion and velocities of the beads at the exterior perimeter of the systems were captured, as previously described,[7] using a tripod-mounted GoPro camera (GoPro, Inc., San Mateo, CA) at a rate of 60 frames per second. The captured images were subsequently analyzed using ImageJ[43] Manual Tracking plugin. Particle velocity relative to bubbles and fixed locations on the bioreactor was calculated iteratively over the course of 1 second. Shear in the absence of bubbles was calculated according to Ramirez, et al., 2003,[44] describing fluid shear on small particles in an RWV bioreactor, as shown in Equation 1,

$$\boldsymbol{\tau = \mu * {|V_F - V_P|}/{a}} \quad (1)$$

where τ is fluid shear stress, μ is the dynamic viscosity of water a 25°C, V_F is the calculated velocity of the water at the particle's radial position if the fluid was acting as a solid body, V_P is the observed velocity of the particle, and a is the radius of the particle.[44] Because the V_F where the fluid encounters the bubble cannot be calculated, the traditional fluid shear formula, Equation 2, was used when a particle interacted with a bubble,

$$\boldsymbol{\tau = \mu * {\delta x}/{\delta y}} \quad (2)$$

where δx is the change in distance (velocity) and δy is the difference in location.[44] Thus, $\delta x/\delta y$ is the velocity gradient developed in the fluid between the wall and the particle. This was repeated for a dose-dependent evaluation of shear and circular fit[45] for bubbles ranging from 0 to 500 µl in the standard bioreactor.

In line with the example of Ramirez at al., 2003, we used Equations 1 and 2, fully cognizant that these are substantial simplifications of the more complex 3D Navier-Stokes equation, the governing equation of motion in fluids.[46–48] All shear values determined from the above equations are reported in dynes/cm^2.

Cell Culture for Morphological Assessment: For cell culture, a new sterilization and conditioning protocol based on an existing HARV protocol was developed and tested[7] This modified protocol is described further in the supplemental section. To assess the morphology of the cell-based organoids/spheroids generated in the RWV under ideal conditions, we paradigmatically used A549 human lung cancer cells (ATCC, Manassas, VA)

Tissue Engineering
An Air Bubble-Isolating Rotating Wall Vessel Bioreactor for Improved Spheroid/Organoid Formation (DOI: 10.1089/ten.TEC.2019.0088)
This paper has been peer-reviewed and accepted for publication, but has yet to undergo copyediting and proof correction. The final published version may differ from this proof.

that have been described extensively in tumor spheroid publications.[49–51] Three ml of complete DMEM were added to each bioreactor, followed by 1 ml of cell suspension at $1x10^6$ cells/ml. The systems were then completely filled with media using 20 ml syringes (BD, Franklin Lakes, NJ) and carefully checked to ensure no bubbles were present. For the novel design, the filling was performed through the valve at the terminal end of the channel. Once cells were added, care was taken to ensure the entrance to the channel was located at the top to prevent cells incidentally entering the channel. Each bioreactor was then mounted on a 4RCCS system (Synthecon), placed inside an incubator (37^0C), and run at 10 rpm, a typical speed for cultures starting as single-cell suspensions in the RWV [7]. After 72 hours, the main volume of each bioreactor was collected into 15 ml conical centrifuge tubes (Corning, Corning, NY). Cells and aggregates were sedimented over 5 minutes and then collected with 1000 µL pipettes. Any standard design HARV bioreactor, which exhibited bubble formation, was excluded from these results so that the impact of bubble formation could be tested under more controlled conditions. Bubbles did also form in the novel BCB design, however, the design performed as intended and no bubbles were observed in the main volume of the BCB in any of our experiments.

In a separate set of studies, air bubbles were intentionally introduced to both the novel and standard bioreactors prior to culture in order to evaluate the effects of bubble formation on A549 aggregate formation and spheroid morphology. The above cell culture steps were followed precisely including the complete filling of the bioreactors with media and removal of air bubbles. Subsequently, an air-filled 1 ml syringe (BD) was attached to one stopcock while an empty 1 ml syringe was attached to the other. Approximately 300 µL of air was added to each bioreactor to simulate a moderate to severe bubble failure. The bioreactors were then operated under precisely the same conditions as the ideal group. The two groups will be referred to as “without bubble” and “with bubble”, respectively. The cell experiment conditions are listed in Supplemental Table 2.

Imaging and Evaluation: For both the “with bubble” and “without bubble” groups, the morphology of the ensuing organoids/spheroids was evaluated by standard image analysis of phase-contrast micrographs. At the end of each culture, the contents of each bioreactor were collected, as described above. Using this method, virtually all aggregates and single cells were collected, which was confirmed by visualizing the supernatant. After

sedimentation, 300 µL of spheroid-containing media was collected from the bottom of the tubes and gently transferred to the 14 mm centers of 35 mm glass-bottom Petri dishes (P35G-1.5-14-C, MatTek, Ashland, MA). At least 10 random images per aliquot were taken at 10X magnification of all available spheroids, aggregates, or individual cells. Images were exported to ImageJ, all identifiable spheroids were manually outlined, and data were recorded on each image for area and circularity. Further information on determining the circularity of the spheroids is provided in the supplementary data section. Aggregates stained for fluorescent live/dead imaging were placed on poly-L-lysine coated MatTek dishes and treated sequentially with 3 µM Calcein AM (Molecular Probes, Eugene, OR) and 3 µM Propidium Iodide (Molecular Probes, Eugene, OR) for 30 minutes each and rinsed three times with PBS before imaging with an FSX100 Fluorescent Microscope (Olympus Life Science, Waltham, MA).

Novel Design Failure Mode Analysis: One possible limitation of this device is the probability of cells entering the channel prior to the establishment of solid-body rotation. To evaluate the probability of this occurrence, Human Dermal Fibroblasts (HDFBs from ATCC) were cultured in complete DMEM (Gibco), as described previously.[52] One hundred thousand HDFBs were added to each of the bioreactors and incubated on the 4RCCS at 10 rpm for 24 hours. HDFBs were selected due to their tendency not to form aggregates, thus reducing error due to changing sedimentation rates. After 24 hours, the media in the main volume and the channel volume were collected into separate conical tubes through the main and the channel ports, respectively, spun down, and resuspended in 1 ml of media. Cell counting was then performed three times on each sample and averages were taken of the totals.

Statistics: Unless stated otherwise, a minimum of three independent experiments (n=3) were performed for each parameter tested. The calculated areas of the organoids/spheroids are presented as medians ± the standard deviation of the medians. Circularity and cell count values are shown as averages ± the standard deviation of the averages. Significance was evaluated with a two-tailed student t-test and results were considered significant with a p-value less than 0.05 after post hoc correction using the Bonferroni method.

Tissue Engineering
An Air Bubble-Isolating Rotating Wall Vessel Bioreactor for Improved Spheroid/Organoid Formation (DOI: 10.1089/ten.TEC.2019.0088)
This paper has been peer-reviewed and accepted for publication, but has yet to undergo copyediting and proof correction. The final published version may differ from this proof.

RESULTS

Design, Modeling, and Computational Fluid Dynamics: Figure 1 shows the design of the novel bioreactor and the results of a computational fluid dynamics analysis, comparing the standard and novel designs under ideal and non-ideal (i.e., in the presence of a bubble) conditions. Panels B, C, E, and F show CFD modeled fluid velocity vectors of the 3D systems viewed from the front. Figures 1B and 1C model the novel bioreactor design without and with a bubble (as indicated by a yellow arrow), respectively. Figures 1E and 1F model the standard design without and with a bubble, respectively. Comparison of Figures 1E and 1F shows that the introduction of a bubble to a standard RWV bioreactor system yields a large high-velocity zone around the bubble that deforms the classic RWV circular fluid paths and creates a noticeable low-velocity eddy directly behind the bubble. For the sake of comparison between the various images, the fluid velocity vector scale bars for all CFD images are shown from 0 m/s to 0.03 m/s. Notably, the red oblong area shown below the bubble in Figure 1F significantly exceeds this range with maximum values in excess of 0.25 m/s. Comparing the results of Figures 1B and 1C to those of Figures 1F and 1E demonstrates the expected physical behavior of the novel design. The results of either condition of the novel design show circular fluid velocity paths that are remarkably similar to that of the standard design under ideal, bubble-free conditions. Figures 1G and 1H demonstrate how a bubble is captured through the channel entrance and Figures 1I and 1J show that the bubbles move towards the back wall of the channel as the novel bioreactor rotates.

Alginate Bead Fluid Dynamics Validation: Figure 2 shows the change in the position of a single alginate bead over one second of rotation of the novel (Figures 2A, 2C) and the standard bioreactor (Figures 2B, 2D), with and without bubbles, after each system had reached equilibrium. The red dots represent the position of that one particle every $1/20^{th}$ of a second (Figures 2A-2D). Shear stress values calculated from Equation 1 are shown in Figures 2E and 2F. Notably, the deflection of the path of the bead in Figure 3D (standard bioreactor with bubble) indicates the fluid dynamic disruption in the RWV by a single bubble and very closely resembles the shape of the fluid velocity vectors in Figure 1F. Though initially the path appears similar to the other three conditions, as soon as the particle interacts with the bubble, it slows, is deflected off of its course, and then

Tissue Engineering
An Air Bubble-Isolating Rotating Wall Vessel Bioreactor for Improved Spheroid/Organoid Formation (DOI: 10.1089/ten.TEC.2019.0088)
This paper has been peer-reviewed and accepted for publication, but has yet to undergo copyediting and proof correction. The final published version may differ from this proof.

accelerated into a new position. This altered movement destroys the condition of whole-body rotation/microgravity simulation due to the disruption of the circular fluid path, while also increasing the maximum shear force as much as five-fold (Figure 2F). The particle paths in Figures 2A-2C closely resemble one another, indicating that the bubble-capturing bioreactor maintains the ideal conditions of zero headspace/whole-body rotation by effectively removing the intentionally introduced bubble. Figures 2E and 2F demonstrate the insignificant differences in both average and maximum shear experienced in the above three "ideal" conditions. Although a bubble is not readily visible in Figure 2C, it is present at the back of the channel (red arrow) and is of the same size as the one in Figure 2D. Figure 2G shows the calculated maximum shear stress of the standard HARV design seeded with bubbles ranging from 25 to 500 µl. All shear results are listed in Supplemental Table 1. The circular residuals resulting from path disruption for various bubble sizes are shown in Supplemental Figure 3. The path disruption images indicate that particles may spend upwards of 25% of their cycle in an abnormal shear state.

Cell Culture: Shown in Figure 3 are representative micrographs of A549 spheroid cultures from each of the four conditions described above for 72 hours. Figures 3A and 3C are representative of typical spheroids from the novel and standard bioreactor without air bubbles while Figures 3B and 3D show the results from BCB and HARV bioreactors initialized with an air bubble. The images in Figures 3A, 3B, and 3C shows similar results in terms of spheroid size and circularity. By contrast, only either small aggregates or single cells were found in the standard bioreactor in the presence of bubbles (Figure 3D). Figures 3E and 3F show fluorescent live/dead staining of aggregates/cells taken from the novel and standard bioreactors respectively when seeded with bubbles. The spheroids taken from the novel bioreactor demonstrate a healthy, live exterior with a "dying core", consistently mirroring the anoxic and subsequently necrotic core of spheroids, as previously demonstrated by others in the RWV.[9] As summarized in Figure 3G introduction of a bubble reduced spheroid area by ~ 10X in a standard bioreactor, but not in the novel design. Interestingly, the circularity of the spheroids was unaffected between the four groups, regardless of condition or spheroid size (3H). Of note, approximately 40% of all experiments performed in the standard design without a bubble were rejected due to

bubbles forming during operation. In our experiments, the BCB design captured and permanently segregated all bubbles within a single rotation after startup.

We also collected the contents of the channels from the novel design bioreactors. While there were generally little to no aggregates nor single cells present, on occasion, a few very large spheroids (typically >500 μm) were found. Phase-contrast microscopy images of typical aggregates found in the BCB channel (Figures 4C and 4D)), demonstrate the large, anisotropic characteristics of aggregates captured in the channel. This may indicate a tendency for larger spheroids to irreversibly enter the channel only once their sedimentation rates exceed the maximum velocity of the rotating media.

Novel Design Failure Mode Analysis: Figure 4 depicts the analysis of the potential failure mode of the novel bioreactor, i.e. of cells irreversibly entering the channel irreversibly (Figure 4A). To assess this possibility, Human Dermal Fibroblasts were seeded into the main volume and cultured for 24 hours, before harvesting and counting the cells to determine the totals in, respectively, the main and channel volumes. As shown in Figure 4B, less than 2% of all cells entered the channel over the course of 24 hours.

DISCUSSION

The aim of this study was to design a modified rotating wall vessel (RWV), capable of producing the same low-shear, microgravity-simulating environment as a typical RWV, while capturing and removing nascent bubbles, thus maintaining the zero-headspace condition, critical to organoid formation. Based on the results shown in Figure 1, we hypothesized that both the standard and novel bioreactor designs would produce similar organoids under bubble-free conditions. However, when a bubble was introduced, organoid formation would be significantly disrupted in the standard bioreactor, while no difference would be observed in the novel BCB. The results in Figures 2 and 3 indeed demonstrate that the modified RWV can produce and maintain the required zero-headspace conditions, while actively removing bubbles and producing large spheroids/organoids, like traditional RWV devices under optimal, bubble-free conditions.

Although the equations used to calculate shear in the alginate bead systems are substantial simplifications, the average experimental values of ~0.04 dynes/cm^2, under ideal conditions, very closely approximated the previously published ideal range of ~0.044

Tissue Engineering
An Air Bubble-Isolating Rotating Wall Vessel Bioreactor for Improved Spheroid/Organoid Formation (DOI: 10.1089/ten.TEC.2019.0088)
This paper has been peer-reviewed and accepted for publication, but has yet to undergo copyediting and proof correction. The final published version may differ from this proof.

Tissue Engineering
An Air Bubble-Isolating Rotating Wall Vessel Bioreactor for Improved Spheroid/Organoid Formation (DOI: 10.1089/ten.TEC.2019.0088)
This paper has been peer-reviewed and accepted for publication, but has yet to undergo copyediting and proof correction. The final published version may differ from this proof.

dynes/cm^2 under zero headspace conditions.[46] By contrast, in the presence of a bubble (Figure 2D), the maximum fluid shear stress increases approximately 10-fold relative to the average to 0.4 dynes/cm^2. This order of magnitude increase appears to be sufficient to disrupt aggregate formation, but may not yet ensure cell damage, which reportedly requires 0.92 dynes/cm^2.[53] When taken contextually with Figure 3D, the appearance of single cells and very small aggregates indicates that spheroid formation was disrupted as a result of increased shear forces. By contrast, the similarity (Figures 3G and 3H) in aggregate sizes in the novel design with and without bubbles indicates that this novel technology achieved its intended goal of reducing the impact of bubbles on aggregate formation. In our use, bubbles did not grow sufficiently large as to overfill the channel or reenter the system over the course of 72 hours. However, should this issue arise with longer-term culture, bubbles can be easily removed from the channel through its Luer port with a simple syringe during operation. Our results demonstrate that the BCB design may combine enhanced reproducibility of organoid generation with improved ease of use and a decreased likelihood of experiment failure. Though the probability of “channel capture” may increase as spheroids grow and sedimentation rates change, this issue can be resolved by increasing the rotational speed of the device.

Our cell culture results taken in conjunction with the shear values obtained with even small bubbles (Figure 2G), demonstrate that the prevention of bubble formation is important for the outcome and reproducibility of experiments using the RWV, yet, it is seemingly underreported in the literature.[30] Because bubble formation is frequent, and its prevention is anecdotal at best, researchers are likely to collect results from RWVs that may intermittently form bubbles (e.g., overnight), not realizing that such an experiment may be compromised. It is one of our intentions that the novel BCB design may be able to prevent false positive/negative results and increase the reproducibility of the system.

While under ideal conditions the calculated shear stresses and the observed cell spheroid sizes were statistically indistinguishable between the "standard without bubble" group and either of the "novel" groups, there are distinct differences between the standard and novel designs. As described in Figure 4, there is a probability of a small subpopulation of the cells irreversibly entering the novel channel during initialization. However, after initialization, channel capture is only likely to occur if the cells or

aggregates tend to drift towards the exterior perimeter of the main volume, with the probability of that tendency increasing if the rotational velocity is incorrect, as seen with the abnormally large aggregates seen in Figures 4C and 4D. In the standard system, a device set to the incorrect speed would still contain all its cell contents. In the novel system, if an incorrect rotational speed is set, aggregates would tend to be captured in the channel, thus providing tangible early feedback that the system settings are inadequate, allowing the speed to be increased as aggregates grow. In a standard system, particles interacting with the wall may be thrown off their circular path, thus negating the modeled microgravity (whole-body rotation, zero headspace) environment. However, these cells would still be collected together with the contents of the entire bioreactor, potentially skewing mechanistic analyses, such as global gene expression profiling in the wake of organoid assembly and differentiation. In the novel system, cells in the channel volume can easily be collected separately and discarded from those in the main volume, ensuring the cells tested are only the ones that did not tend towards the wall, decreasing skew and increasing the consistency of results.

In summary, we engineered and tested a modification to the traditional HARV-type rotating wall vessel bioreactor, which results in the effective capture and removal of bubbles. In this paper, we compared the modified BCB and standard HARV bioreactors side by side and found similarities in both fluid dynamics and in the ability to generate sizeable cancer spheroids in the absence of bubbles. However, in the presence of a bubble, the spheroid/organoid formation is impaired in conventional RWVs, while it is fully maintained in the modified design. We anticipate that the novel design will increase experimental reproducibility and consistency when using these kinds of rotatory bioreactors.

DISCLOSURE STATEMENT: Temple University has filed a patent application for the novel bioreactor design, with MAP and PIL as named co-inventors.

Tissue Engineering
An Air Bubble-Isolating Rotating Wall Vessel Bioreactor for Improved Spheroid/Organoid Formation (DOI: 10.1089/ten.TEC.2019.0088)
This paper has been peer-reviewed and accepted for publication, but has yet to undergo copyediting and proof correction. The final published version may differ from this proof.

ACKNOWLEDGMENTS: The authors wish to thank Mr. Robert Redden and Mrs. Helen Freitas (Dept. Bioengineering) for their guidance and support. Thanks to Kelsey Manahan-Phelan (Library and Archives, Academy of Natural Sciences, Philadelphia) for her assistance in sourcing references. Our research is supported by the National Aeronautics and Space Agency (NASA), Grant # 80NSSC18K1480 and the Intramural Research Program of the National Eye Institute (EY000450, EY000
474, EY000546).

References

1. Antoni D, Burckel H, Josset E, Noel G. Three-dimensional cell culture: a breakthrough in vivo. *Int J Mol Sci*. 2015;16(3):5517-5527. doi:10.3390/ijms16035517
2. Xinaris C, Brizi V, Remuzzi G. Organoid Models and Applications in Biomedical Research. *Nephron*. 2015;130(3):191-199. doi:10.1159/000433566
3. Fang Y, Eglen RM. Three-Dimensional Cell Cultures in Drug Discovery and Development. *SLAS Discov Adv life Sci R D*. 2017;22(5):456-472. doi:10.1177/1087057117696795
4. Eder T, Eder IE. 3D Hanging Drop Culture to Establish Prostate Cancer Organoids. In: Humana Press, New York, NY; 2017:167-175. doi:10.1007/978-1-4939-7021-6_12
5. Lelkes PI, Galvan DL, Thomas Hayman G, et al. Simulated microgravity conditions enhance differentiation of cultured PC12 cells towards the neuroendocrine phenotype. *Vitr Cell Dev Biol - Anim*. 1998;34(4):316-325. doi:10.1007/s11626-998-0008-y
6. Gerecht-Nir S, Cohen S, Itskovitz-Eldor J. Bioreactor Cultivation Enhances the Efficiency of Human Embryoid Body (hEB) Formation and Differentiation. 2004. doi:10.1002/bit.20045
7. Botta GP, Manley P, Miller S, Lelkes PI. Real-time assessment of three-dimensional cell aggregation in rotating wall vessel bioreactors in vitro. *Nat Protoc*. 2006;1(5):2116-2127. doi:10.1038/nprot.2006.311
8. Redden RA, Doolin EJ. Microgravity assay of neuroblastoma: in vitro aggregation kinetics and organoid morphology correlate with MYCN expression. 2011. doi:10.1007/s11626-011-9393-8
9. Redden RA, Iyer R, Brodeur GM, Doolin EJ. Rotary bioreactor culture can discern specific behavior phenotypes in Trk-null and Trk-expressing neuroblastoma cell lines. *Vitr CelL Dev Biol*. 2014. doi:10.1007/s11626-013-9716-z
10. Radtke AL, Herbst-Kralovetz MM. Culturing and Applications of Rotating Wall Vessel Bioreactor Derived 3D Epithelial Cell Models. *J Vis Exp*. 2012;62379138683868(10):3868-103791. doi:10.3791/3868

11. Mattei C, Alshawaf A, D 'abaco G, Nayagam B, Dottori M. Generation of Neural Organoids from Human Embryonic Stem Cells Using the Rotary Cell Culture System: Effects of Microgravity on Neural Progenitor Cell Fate. *Stem Cells Dev*. 2018. doi:10.1089/scd.2018.0012

12. Qian X, Jacob F, Song MM, Nguyen HN, Song H, Ming G. Generation of human brain region–specific organoids using a miniaturized spinning bioreactor. *Nat Protoc*. 2018;13(3):565-580. doi:10.1038/nprot.2017.152

13. Villa A, Versari S, Maier JAM, Bradamante S. Cell behavior in simulated microgravity: a comparison of results obtained with RWV and RPM. *Gravitational Sp Biol*. 2005;18(2):89-91.

14. Catapano G, Speranza G, Maniglio D, DeBartolo L, Della Volpe C. Bioreactor type and operating conditions influence cell response to polymeric material properties. In: *Proceedings of the IEEE-EMBS Special Topic Conference on Molecular, Cellular and Tissue Engineering*. IEEE; 2002:60-61. doi:10.1109/MCTE.2002.1175004

15. Wells A, Rodrigues M, Wells AW, Nuschke A. Starvation as an Initiator of Mesenchymal Stem Cell/ Multipotent Stromal Cell Differentiation. *J Stem Cell Res Ther*. 2016;1(3). doi:10.15406/jsrt.2016.01.00020

16. Dahan P, Lu V, Nguyen RMT, Kennedy SAL, Teitell MA. Metabolism in pluripotency: Both driver and passenger? *J Biol Chem*. 2019;294(14):5420-5429. doi:10.1074/jbc.TM117.000832

17. Hubert CG, Rivera M, Spangler LC, et al. A Three-Dimensional Organoid Culture System Derived from Human Glioblastomas Recapitulates the Hypoxic Gradients and Cancer Stem Cell Heterogeneity of Tumors Found *In Vivo*. *Cancer Res*. 2016;76(8):2465-2477. doi:10.1158/0008-5472.CAN-15-2402

18. Forristal CE, Wright KL, Hanley NA, Oreffo ROC, Houghton FD. Hypoxia inducible factors regulate pluripotency and proliferation in human embryonic stem cells cultured at reduced oxygen tensions. *Reproduction*. 2010;139:85-97. doi:10.1530/REP-09-0300

19. Ayabe H, Anada T, Kamoya T, et al. Optimal Hypoxia Regulates Human iPSC-Derived Liver Bud Differentiation through Intercellular TGFB Signaling. *Stem cell reports*. 2018;11(2):306-316. doi:10.1016/j.stemcr.2018.06.015

20. Grebenyuk S, Ranga A. Engineering Organoid Vascularization. *Front Bioeng Biotechnol*. 2019;7:39. doi:10.3389/fbioe.2019.00039

21. Wang Y, Wang L, Guo Y, Zhu Y, Qin J. Engineering stem cell-derived 3D brain organoids in a perfusable organ-on-a-chip system. *RSC Adv*. 2018;8(3):1677-1685. doi:10.1039/C7RA11714K

22. Wolfe RP, Ahsan T. Shear stress during early embryonic stem cell differentiation promotes hematopoietic and endothelial phenotypes. *Biotechnol Bioeng*. 2013;110(4):1231-1242. doi:10.1002/bit.24782

23. Regmi S, Fu A, Luo KQ. High Shear Stresses under Exercise Condition Destroy Circulating Tumor Cells in a Microfluidic System. *Sci Rep*. 2017;7(1):39975. doi:10.1038/srep39975

24. Ovando-Roche P, West EL, Branch MJ, et al. Use of bioreactors for culturing human retinal organoids improves photoreceptor yields. *Stem Cell Res Ther*. 2018;9(1):156. doi:10.1186/s13287-018-0907-0

25. Frangos JA, McIntire L V, Eskin SG. Shear stress induced stimulation of mammalian cell metabolism. *Biotechnol Bioeng*. 1988;32(8):1053-1060. doi:10.1002/bit.260320812

26. Poli D, Magliaro C, Ahluwalia A. Experimental and Computational Methods for the Study of Cerebral Organoids: A Review. *Front Neurosci*. 2019;13:162. doi:10.3389/fnins.2019.00162

27. DiStefano T, Chen HY, Panebianco C, et al. Accelerated and Improved Differentiation of Retinal Organoids from Pluripotent Stem Cells in Rotating-Wall Vessel Bioreactors. *Stem cell reports*. 2018;10(1):300-313. doi:10.1016/j.stemcr.2017.11.001

28. Phelan MA, Lelkes PI, Swaroop A. Mini and customized low-cost bioreactors for optimized high-throughput generation of tissue organoids. *Stem Cell Investig*. 2018. doi:10.21037/sci.2018.09.06

29. Schwarz RP, Goodwin TJ, Wolf DA. Cell culture for three-dimensional modeling in rotating-wall vessels: An application of simulated microgravity. *J Tissue Cult Methods*. 1992;14(2):51-57. doi:10.1007/BF01404744

30. Hammond TG, Hammond JM. Optimized suspension culture: the rotating-wall vessel. *Am J Physiol Renal Physiol*. 2001. doi:10.1152/ajprenal.2001.281.1.F12

31. Hammond T, Allen P, Birdsall H. Is There a Space-Based Technology Solution to Problems with Preclinical Drug Toxicity Testing? *Pharm Res*. 2016;33(7):1545-1551. doi:10.1007/s11095-016-1942-0

32. King JA, Miller WM. Bioreactor Development for Stem Cell Expansion and Controlled Differentiation. *Curr Opin Chem Biol*. 2007;11(4):394. doi:10.1016/J.CBPA.2007.05.034

33. Pollack SR, Meaney DF, Levine EM, Litt M, Johnston ED. Numerical Model and Experimental Validation of Microcarrier Motion in a Rotating Bioreactor. *TISSUE Eng*. 2000;6(5).

34. Salerno-Goncalves R, Fasano A, Sztein MB. Development of a Multicellular Three-dimensional Organotypic Model of the Human Intestinal Mucosa Grown Under Microgravity. *J Vis Exp*. 2016;(113). doi:10.3791/54148

35. Varley MC, Markaki AE, Brooks RA. Effect of Rotation on Scaffold Motion and Cell Growth in Rotating Bioreactors. *Tissue Eng Part A*. 2017;23(11-12):522-534. doi:10.1089/ten.TEA.2016.0357

36. Wuest SL, Richard S, Kopp S, Grimm D, Egli M. Simulated microgravity: critical review on the use of random positioning machines for mammalian cell culture. *Biomed Res Int*. 2015;2015:971474. doi:10.1155/2015/971474

37. Niederhaus C, Nahra H, Gonda S, et al. Bubble Experiments on the Hydrodynamic Focusing Bioreactor-Space (HFB-S). In: New London, CT, USA: Gordon Conference on Gravitational Effects on Physico-Chemical Systems; 2002. https://ntrs.nasa.gov/search.jsp?R=20040000164. Accessed June 27, 2019.

38. Lelkes PI, Unsworth BR. Neuroectodermal Cell Culture. In: *Methods of Tissue Engineering*. Elsevier; 2002:371-382. doi:10.1016/B978-012436636-7/50144-0

39. Sanford GL, Ellerson D, Melhado-Gardner C, Sroufe AE, Harris-Hooker S. *Three-Dimensional Growth of Endothelial Cells in the Microgravity-Based Rotating Wall*. Vol 38.; 2002. doi:10.1290/1071-

40. Choi CK, Helmke BP. Short-Term Shear Stress Induces Rapid Actin Dynamics in Living Endothelial Cells. *Mol Cell Biomech*. 2008;5(4):247-258. doi:10.1002/term.1493

41. Yu-shuang L, Jiong C. Moisture vapor transmission rates of various transparent dressings at different temperatures and humidities. *Chin Med J (Engl)*. 2009;122(8):927-930. doi:10.3760/cma.j.issn.0366-6999.2009.08.009

42. Botchwey EA, Pollack SR, Levine EM, Laurencin CT. Bone tissue engineering in a rotating bioreactor using a microcarrier matrix system. *J Biomed Mater Res*. 2001;55(2):242-253. doi:10.1002/1097-4636(200105)55:2<242::AID-JBM1011>3.0.CO;2-D

43. Schindelin J, Arganda-Carreras I, Frise E, et al. Fiji: an open-source platform for biological-image analysis. *Nat Methods*. 2012;9(7):676-682. doi:10.1038/nmeth.2019

44. Ramirez LES, Lim EA, Coimbra CFM, Kobayashi MH. On the dynamics of a spherical scaffold in rotating bioreactors. *Biotechnol Bioeng*. 2003;84(3):382-389. doi:10.1002/bit.10778

45. Brown R. fitcircle.m. MATLAB Central File Exchange. https://www.mathworks.com/matlabcentral/fileexchange/15060-fitcircle-m. Accessed June 28, 2019.

46. Begley CM, Kleis SJ. The Fluid Dynamic and Shear Environment in the NASA/JSC Rotating-Wall Perfused-Vessel Bioreactor. *Biotechnol Bioeng*. 2000;70:32-40.

47. Munson, Okiishi, Huebsch, Rothmayer. *Fluid Mechanics*. 7th ed. John Wiley & Sons, Inc.; 2012. www.wileyplus.com. Accessed August 2, 2018.

48. Wolf DA, Schwarz RP. Analysis of gravity-induced particle motion and fluid perfusion flow in the NASA-designed rotating zero-head-space tissue culture vessel. October 1991. https://ntrs.nasa.gov/search.jsp?R=19920004122. Accessed May 28, 2018.

49. Sambale F, Lavrentieva A, Stahl F, et al. Three dimensional spheroid cell culture for nanoparticle safety testing. *J Biotechnol*. 2015;205:120-129. doi:10.1016/J.JBIOTEC.2015.01.001

50. Zuchowska A, Jastrzebska E, Chudy M, Dybko A, Brzozka Z. 3D lung spheroid cultures for evaluation of photodynamic therapy (PDT) procedures in microfluidic Lab-on-a-Chip system. *Anal Chim Acta*. 2017;990:110-120. doi:10.1016/J.ACA.2017.07.009

51. Maruhashi R, Akizuki R, Sato T, et al. Elevation of sensitivity to anticancer agents of human lung adenocarcinoma A549 cells by knockdown of claudin-2 expression in monolayer and spheroid culture models. *Biochim Biophys Acta - Mol Cell Res*. 2018;1865(3):470-479. doi:10.1016/J.BBAMCR.2017.12.005

52. Lin L, Perets A, Har-El Y-E, et al. *Alimentary "green" Proteins as Electrospun Scaffolds for Skin Regenerative Engineering*.; 2012. doi:10.1002/term.1493

53. Goodwin TJ, Prewett TL, Wolf DA, Spaulding GF. Reduced shear stress: A major component in the ability of mammalian tissues to form three-dimensional assemblies in simulated microgravity. *J Cell Biochem*. 1993;51(3):301-311. doi:10.1002/jcb.240510309

Figure Legends

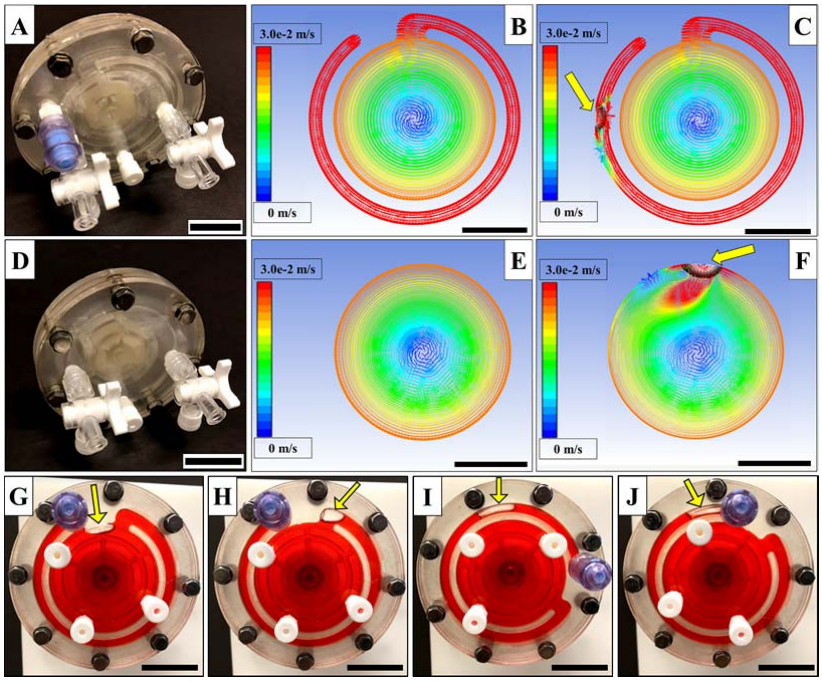

Figure 1. Fabrication and Modeling of the Novel and Standard Bioreactor – (A) A fully assembled novel bioreactor. (B, C) A front-viewed 3D model of stable fluid velocity vectors in a novel design bioreactor without bubbles and with, respectively. Note: the bubble highlighted by the arrow is trapped in the channel without disrupting the velocity gradient in the main chamber. (D) A fully assembled standard bioreactor. (E, F) A front-viewed 3D model of stable fluid velocity vectors in a standard design bioreactor without bubbles and with, respectively. Note the significant increase in fluid velocity (exceeding the velocity scale by ~ 10-fold, see text) after encountering the bubble (yellow arrow). (G-J) Photographs of the movement of an actual bubble (yellow arrow) in the novel design highlighted by red colored liquid. (G, H) Bubble entering the channel. (I, J) A bubble moving through the channel to the back wall. All scale bars are 2.5 cm.

Tissue Engineering
An Air Bubble-Isolating Rotating Wall Vessel Bioreactor for Improved Spheroid/Organoid Formation (DOI: 10.1089/ten.TEC.2019.0088)
This paper has been peer-reviewed and accepted for publication, but has yet to undergo copyediting and proof correction. The final published version may differ from this proof.

Tissue Engineering
An Air Bubble-Isolating Rotating Wall Vessel Bioreactor for Improved Spheroid/Organoid Formation (DOI: 10.1089/ten.TEC.2019.0088)

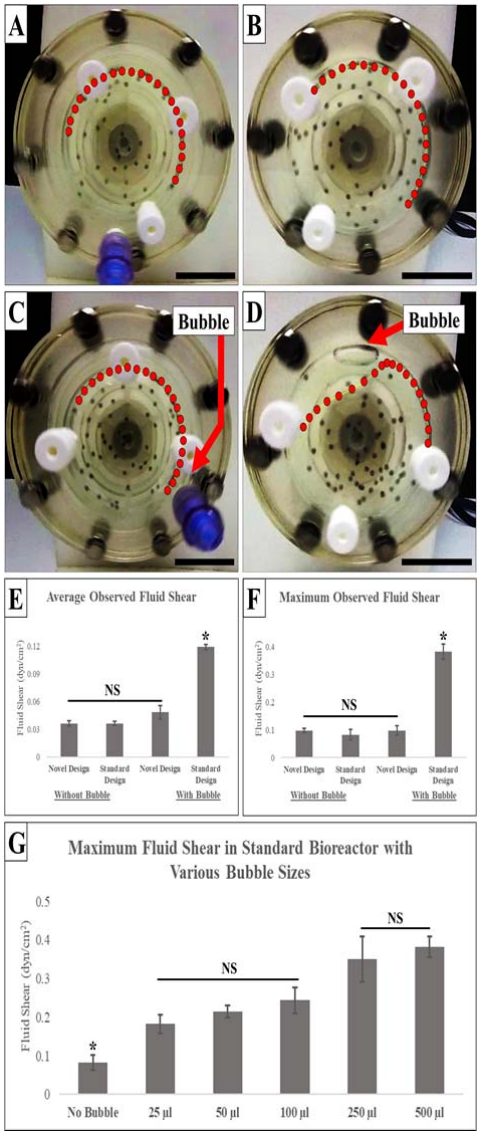

Figure 2. Alginate Bead Shear Modeling - (A-D) The position (tracked in red) of alginate beads over one second marked every 1/20th of a second in RWV bioreactors rotating counter-clockwise under the four conditions defined in Figure 2G-2H. The bubble is shown by the red arrows in C and D. (E) The average fluid shear stress experienced by the beads over the course of the path. The shear stress in the novel design with bubbles is not significantly different from that in the first two instances. (F) The maximum shear stress experienced by the beads during the observed path. (G) Maximum shear values observed in the standard bioreactor with increasing bubble size. Shear stress measurements are detailed in the text. All scale bars are 2.5 cm.

Tissue Engineering
An Air Bubble-Isolating Rotating Wall Vessel Bioreactor for Improved Spheroid/Organoid Formation (DOI: 10.1089/ten.TEC.2019.0088)
This paper has been peer-reviewed and accepted for publication, but has yet to undergo copyediting and proof correction. The final published version may differ from this proof.

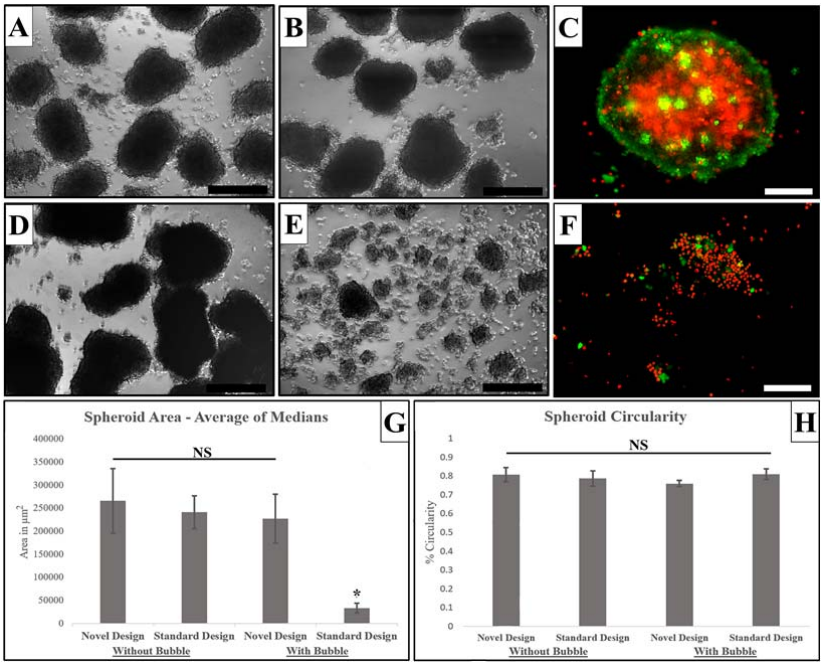

Figure 3. A549 Cell Culture Results for Spheroid Morphology after 72 Hours - (A) Spheroid formation in the novel design with no bubble present. (B) Spheroid formation in the standard design with no bubble present. (C) Calcein AM/Propidium Iodide (green/red respectively) staining of a spheroid from the novel design with a bubble present. (D) Spheroid formation in the novel design with a bubble present. (E) Spheroid formation in the standard design with a bubble present. (F) Calcein AM/Propidium Iodide (green/red respectively) staining of a spheroid from the standard design with a bubble present. (G) Combined quantified results for spheroid areas for each of the above conditions taken as the average of medians, for details, see text. (H) Combined quantified results for spheroid circularity taken as an average of averages of independent triplicate data, for details, see text. Scale bars for A, B, D, E are 200 µm, scale bars for C and F are 100 µm.

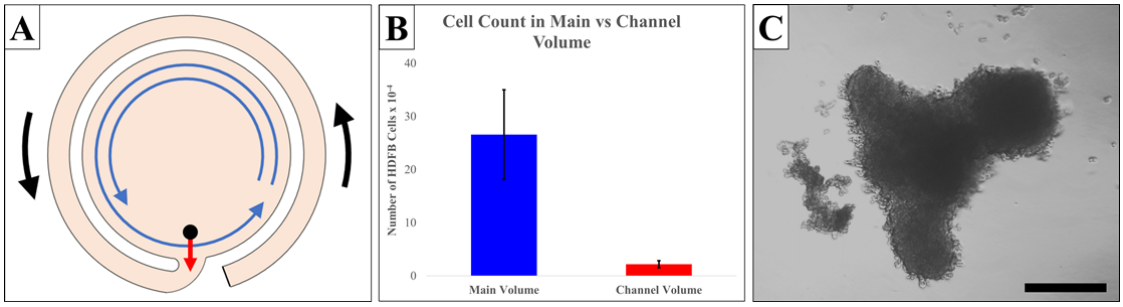

Figure 4. Experimental Analysis of a Failure Mode - (A) Conceptual representation of the path by which the "channel capture" failure mode may occur during initialization of reactor rotation. (B) Experimental validation: the incidence of channel capture of human dermal fibroblasts cultured for 24 hours. Those retained in the main volume are shown in blue and those captured by the channel are shown in red. (C) Representative images of A549 aggregates of aggregates taken from the channel volume of the novel bioreactor after 72 hours in culture. Scale bar for C is 200 µm.

Tissue Engineering
An Air Bubble-Isolating Rotating Wall Vessel Bioreactor for Improved Spheroid/Organoid Formation (DOI: 10.1089/ten.TEC.2019.0088)

Device Fabrication Details:

There were three primary pieces for each bioreactor. A front plate served to close the system and to provide holes for the addition of filling and emptying ports by tapping 1/4”-28 holes and connecting to screw-to-Luer Lock Quick Turn Couplings (McMaster-Carr, Elmhurst, IL). The front plate of the novel bioreactors contained an additional port at the terminal end of the channel fitted with a pressure activated Luer valve for filling and bubble removal. A central acrylic ring served as the perimeter wall for the fluid, with the novel variants containing the bubble catch channel. The back wall served as a vented backing for gas perfusion and as an anchor point for attachment to a rotation system via a 5/8”-11 nylon nut (McMaster-Carr). All acrylic pieces were pre-cut to accept M4 bolt holes around their perimeter for assembly. After taping to add thread, all acrylic pieces were annealed in an 85°C oven and gradually cooled to RT. Finally, the pieces were assembled in the following order: front acrylic plate, silicone gasket, central acrylic ring, silicone gasket, gas-permeable membrane (Tegaderm facing central ring), back acrylic plate, nylon nut. The assembled bioreactor was held together with M4x16 bolts with two flat washers, one spring washer, and one nut each.

Device Dimensions:

Common Dimensions:

Acrylic Thickness: 4.2 mm

Gasket Silicone Thickness: 0.5 mm

Membrane thickness:0.2mm

Coupling Nut Type: 5/8”-11

Total Thickness: 14.5 mm

Main Volume Diameter: 50 mm

Standard Bioreactor Specifications:

Total Volume: 10 mL

Outer Diameter: 76 mm

Bubble-Catching Bioreactor Specifications:

Total Volume: 13 mL

Main Chamber Volume: 10 mL

Channel Volume: 3 mL

Tissue Engineering
An Air Bubble-Isolating Rotating Wall Vessel Bioreactor for Improved Spheroid/Organoid Formation (DOI: 10.1089/ten.TEC.2019.0088)
This paper has been peer-reviewed and accepted for publication, but has yet to undergo copyediting and proof correction. The final published version may differ from this proof.

Interior Diameter (Channel): 66 mm (Channel diameter: 3.8mm)

Channel Entrance Width: 8 mm

Channel Wall Thickness: 3 mm

Outer Diameter: 87 mm

CFD Details, Boundary Conditions, and Settings:

For models not containing bubbles, the following settings were used:

Solver: Type = Pressure-based

Model: Multiphase = Off, Viscous = laminar, Energy = Off (Incompressible).

Shear condition: No Slip

Fluid: water (default), Density = 998.2 kg/m^3, Viscosity = 0.001003 kg/m^{-s}

3D depth of the design: 4.8 mm

For models containing bubbles, the following settings were used:

Solver: Type = Pressure-based

Model: Multiphase = Eulerian (Phase Interaction – Wall Lubrication = antal-et-al, Surface Tension = 0.07, Viscous = laminar, Energy = Off (Incompressible).

Shear condition: No Slip

Fluid (Phase 1): water (default), Density = 998.2 kg/m^3, Viscosity = 0.001003 kg/m^{-s}

Fluid (Phase 2): water-vapor (default), Density = 0.5542kg/m^3, Viscosity = 1.34e^{-05} kg/m^{-s}

3D depth of the design: 4.8 mm

Simulations were run at 1 G and at a rotational speed of 10 rpm. The shown computed results were obtained at a node length of 1.0 mm and a time step of 0.01 seconds. Grid- and time-independent analyses were performed by verifying the observed dynamics at a node size of 0.325 mm (approximately 500,000 nodes per simulation) and a time step of 0.005 seconds, respectively (see Supplementary Figure 1). All four CFD simulation conditions were also run with the laminar viscous model substituted for the k-epsilon (2 eqn) model with no observable change in results. Both non-bubble conditions

Tissue Engineering
An Air Bubble-Isolating Rotating Wall Vessel Bioreactor for Improved Spheroid/Organoid Formation (DOI: 10.1089/ten.TEC.2019.0088)

were run with the Eulerian multiphase model, described above, with no observable difference in the results from multiphase: off. Additionally, both bubble containing simulations were run with both water vapor bubbles and dry air bubbles. The changes in the type of gaseous material did not yield observable differences in the results. Finally, all four conditions were run with a Volume of Fluid multiphase model. For the "no-bubble" conditions, there was no observable change. For the "with bubble" conditions, the shapes of the gas bubbles less closely resembled the empirical observations than the Eulerian model. Irrespective of the close similarity between empirical observations and numerical prediction, the Eulerian model was chosen for our simulations to assess the probability of a bubble splitting or "frothing" when encountering the edge of the channel wall while entering the channel in the novel design, of which, none was observed. Water vapor was chosen over dry air to more closely simulate the very high humidity environment of incubators and subsequently bubbles that form at liquid interfaces in them. Preliminary results indicated that performing the simulations at various speeds from 5 rpm to 25 rpm did not affect the calculated relative velocities or fluid paths (not shown).

Alginate Bead Experiment Details:

Alginate beads were produced by dropwise adding a (w/v) aqueous mix of 0.75% sodium alginate (Sigma-Aldrich, St. Louis, MO), 1% polyethylene oxide (Sigma-Aldrich, St. Louis, MO), and 2% powdered charcoal (for color) into a stirred 2% calcium chloride bath. All shear values obtained are reported in Supplemental Table 1.

Explanation of the Circularity Equation for Figure 3:

The circularity value reported in Figure 3H is an output value using the ImageJ "Circularity" function. After each spheroid had its perimeter traced, the software automatically calculated the total perimeter and total area of each image. The circularity function outputs a value according to the equation below:

$$circularity = 4\pi(area/perimeter^2)$$

This generates a value between 0 and 1 which gives an estimate of how circular a 2D object is. We chose to report this value to demonstrate that the modified design did not substantially change spheroid morphology. Had this been the case, spheroids may have been observed as significantly ellipsoid from spinning on their longer axis for a higher

percentage of the time, aggregating into larger, amorphous shapes, or being torn into random, pointed shapes. Our data suggest none of these is the case.

Cell Culture Details:

To sterilize and condition the bioreactors, each was filled with 0.2 N NaOH for 24 hours. All bioreactors were then moved to a laminar flow hood and exposed to UV sterilization for 30 minutes on each side. They were then emptied of the NaOH and rinsed three times with sterile 1x PBS (Corning, Corning, NY). Next, the bioreactors were filled with a sterile conditioning solution composed of 10% FBS (Gibco, Gaithersburg, MD), 88% 1x PBS (Corning, Corning, NY), and 2% Penicillin-Streptomycin (Pen-Strep, Gibco, Gaithersburg, MD) and incubated at 37°C for 24 hours while rotating at 10 rpm on a 4RCCS rotary system (Synthecon, Inc., Houston, TX). After conditioning, the bioreactors were emptied aseptically and immediately used for cell culture. Cells were maintained in a T75 flask (Falcon) in DMEM (Gibco) supplemented with 10% FBS, 1% Pen-Strep, and 1% L-glutamine (Gibco). Once the cultures reached ~80-90% confluence, cells were rinsed with PBS and detached using 1x Trypsin (Gibco) and resuspended in DMEM at a concentration of 1x 10^6 cells/ml. A brief description of experimental conditions is shown in Supplemental Table 2.

Supplemental Table 1 – All Maximum and Average Shear Values:

	Max Shear (dynes/cm^2)	Average Shear (dynes/cm^2)
BCB - No Bubble	0.098 ± 0.007	0.036 ± 0.003
BCB - 500 µl Bubble	0.098 ± 0.017	0.048 ± 0.007
Standard - No Bubble	0.082 ± 0.019	0.036 ± 0.002
Standard - 25 µl Bubble	0.183 ± 0.024	0.081 ± 0.010
Standard - 50 µl Bubble	0.215 ± 0.016	0.100 ± 0.016
Standard - 100 µl Bubble	0.244 ± 0.033	0.119 ± 0.011
Standard - 250 µl Bubble	0.350 ± 0.058	0.159 ± 0.015
Standard - 500 µl Bubble	0.382 ± 0.027	0.119 ± 0.002

Tissue Engineering
An Air Bubble-Isolating Rotating Wall Vessel Bioreactor for Improved Spheroid/Organoid Formation (DOI: 10.1089/ten.TEC.2019.0088)
This paper has been peer-reviewed and accepted for publication, but has yet to undergo copyediting and proof correction. The final published version may differ from this proof.

Supplemental Table 2 – A Description of Cell Experiment Conditions:

	Novel BCB without Bubble	Novel BCB with Bubble	Standard HARV-type without Bubble	Standard HARV-type with Bubble
Bubble Size	0 µl	300 µl	0 µl	300 µl
Initial Cell Density	100,000 cells/ml	100,000 cells/ml	100,000 cells/ml	100,000 cells/ml
Rotational Speed	10 rpm	10 rpm	10 rpm	10 rpm
Culture time	72 hours	72 hours	72 hours	72 hours
n =	10	10	8	11
# Rejected	0	0	5	0

Tissue Engineering
An Air Bubble-Isolating Rotating Wall Vessel Bioreactor for Improved Spheroid/Organoid Formation (DOI: 10.1089/ten.TEC.2019.0088)

Tissue Engineering
An Air Bubble-Isolating Rotating Wall Vessel Bioreactor for Improved Spheroid/Organoid Formation (DOI: 10.1089/ten.TEC.2019.0088)

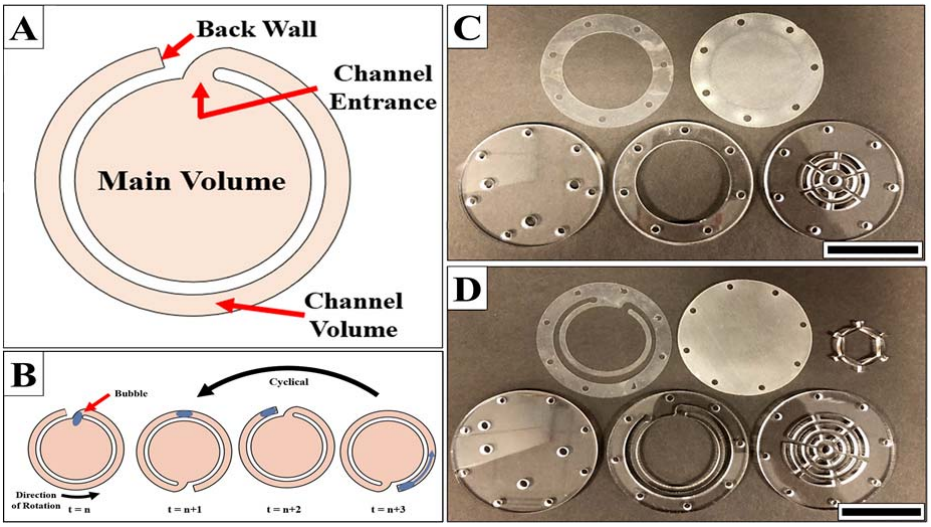

Supplemental Figure 1. Design and Fabrication of the Bioreactors – (A) A description of key parts of the novel BCB design. (B) A description of how bubbles are captured and isolated in the novel BCB. (C) The laser-cut components of the replicated standard design. (D) The laser-cut components of the novel BCB design. Scale bars are 5 cm.

Tissue Engineering
An Air Bubble-Isolating Rotating Wall Vessel Bioreactor for Improved Spheroid/Organoid Formation (DOI: 10.1089/ten.TEC.2019.0088)
This paper has been peer-reviewed and accepted for publication, but has yet to undergo copyediting and proof correction. The final published version may differ from this proof.

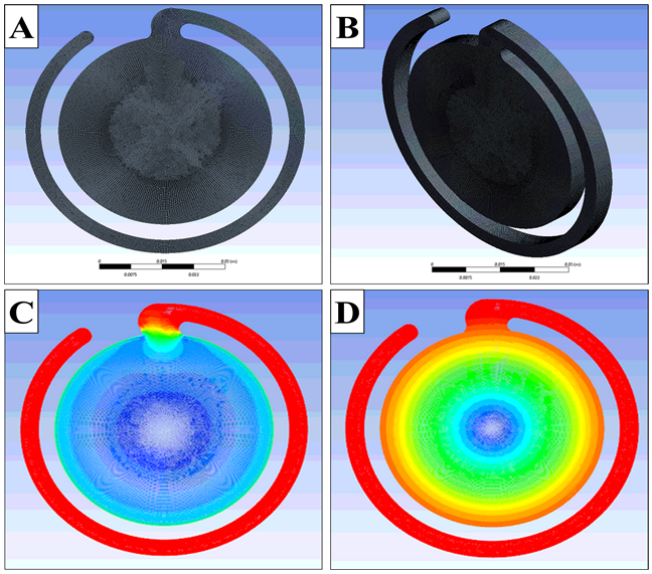

Supplemental Figure 2. **Set of grid-independent validations performed on the modified, bubble capturing design at a node size of 0.325 mm -** (A) A front-facing view of the CFD mesh in the novel BCB. (B) An isometric view of the mesh. (C) The CFD fluid velocity vectors after 0.01 seconds. (D) The fluid velocity vectors after stabilization. All scale bars are 3 cm.

Tissue Engineering
An Air Bubble-Isolating Rotating Wall Vessel Bioreactor for Improved Spheroid/Organoid Formation (DOI: 10.1089/ten.TEC.2019.0088)
This paper has been peer-reviewed and accepted for publication, but has yet to undergo copyediting and proof correction. The final published version may differ from this proof.

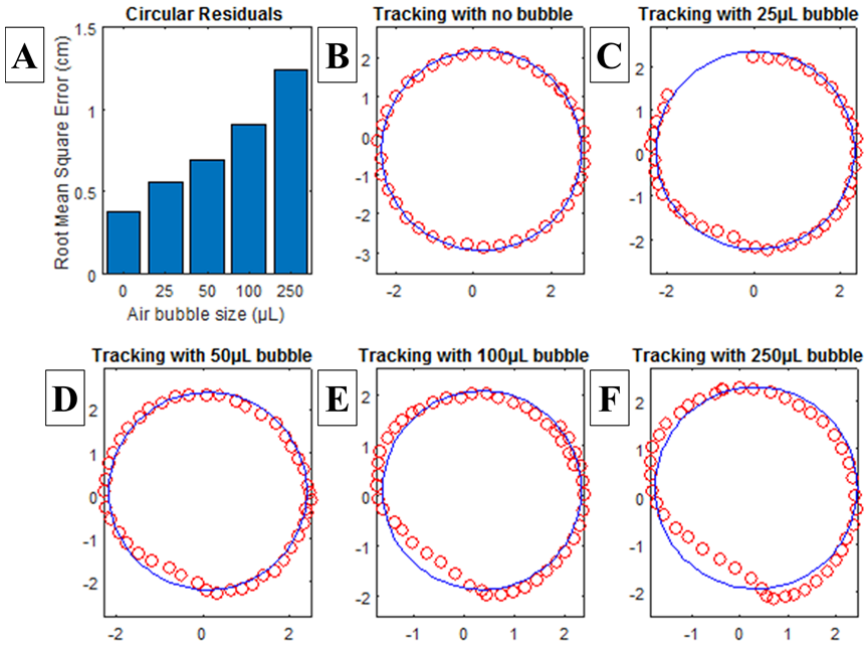

Supplemental Figure 3. Dose-Dependent Effects of Bubbles on Bioreactor Behavior – (A) The circular residuals of tracked alginate particle motion to represent the degree of deflection when encountering bubbles of various sizes. (B-F) Graphing representation of the tracked alginate particle data fit against a circle to obtain residuals.